Short Communication
Quantification of loess proportions in Pleistocene periglacial slope deposits and Holocene colluvium using grain-size data by laser diffractometry

Fei Yang[1,2*], **Volker Karius**[3], and **Daniela Sauer**[2]

[1] Institute of Soil Science, Chinese Academy of Sciences, Nanjing, China
[2] Department of Physical Geography, University of Göttingen, Göttingen, Germany
[3] Department of Sedimentology and Environmental Geology, University of Göttingen, Göttingen, Germany

Abstract

Loess proportions in slope deposits have rarely been quantified, due to the lack of quantification methods. In this study, we used laser granulometry to analyze grain-size distributions in slope deposits of a Buntsandstein landscape in central Germany. The consistent loess contents obtained from two independent models corroborate the validity of the calculated loess proportions and the applicability of the new R package EMMAgeo. Yet, some limitations in transferability need to be considered.

Key words: EMMAgeo / grain-size distribution / loess / Pleistocene periglacial slope deposits

Accepted March 12, 2020

1 Introduction

Loess admixture plays an important role in the formation of Pleistocene periglacial slope deposits (PPSD) in many midlatitude regions (*Kleber*, 1997; *Semmel* and *Terhorst*, 2010), *e.g*., in Germany (*Sauer* and *Felix-Henningsen*, 2004; *Raab* et al., 2007), Poland (*Waroszewski* et al., 2019), Switzerland (*Mailänder* and *Veit*, 2001), and the United States (*Krautz* et al., 2018). Although numerous studies have reported typical magnitudes of loess admixture in the different types of PPSD (*Kleber* and *Terhorst*, 2013), the quantification of loess proportions in PPSD still remains a challenge, due to a lack of suitable quantification methods. Grain-size distribution (GSD) is commonly used to estimate loess addition to sediments and soils, as loess typically has silty texture. However, so far these estimates are rather qualitative and descriptive than quantitative, as the resolution of GSD data obtained from the classical sieve and pipette method is not sufficient for use in a quantitative approach. In comparison, laser diffraction generates more detailed and quantifiable data on GSD. Thus, it has been widely adopted for numerical analysis in sedimentology and related disciplines. In addition, several functions have been proposed to quantify subpopulations of mixed sediments by decomposing multi-modal GSDs (*e.g*., *Weltje*, 1997; *Sun* et al., 2002; *Paterson* and *Heslop*, 2015). One of the most widely used algorithms is the nonparametric endmember modelling analysis (EMMA), which is capable of producing endmember loadings and endmember scores, based on Eigen-space analysis and compositional data constrains (*Dietze* et al., 2012). The recently published R package 'EMMAgeo' provides a set of functions for endmember modelling analysis (EMMA) of grain size data (*Dietze* and *Dietze*, 2019). Whether this method can be applied to determine loess proportions in soils still needs further exploration. In this study, we tested the suitability of GSD data obtained by laser diffraction to quantify loess proportions in soils developed in PPSD. For this test, we used both the deterministic EMMA approach and a simple two-endmembers unmixing model.

2 Material and methods

2.1 Study area and sampling

The study area is in central Germany, 10 km east of Göttingen (near Ebergötzen). We sampled 17 soil profiles in various topographic positions along a small valley (ca. 1 km long and up to 0.5 km wide), running from west to east. The valley is carved into Lower Triassic sandstone (Buntsandstein), overlain by PPSD and Holocene colluvium (HC, here broadly defined as Holocene slope deposits translocated by gravitation and unconcentrated runoff; *Kleber*, 2006). All pedons were sampled horizon-wise. Different layers of PPSD, *i.e*., upper layer (UL), intermediate layer (IL), and basal laser (BL) were classified according to the German substrate taxonomy (*AK Bodensystematik*, 1998). Moreover, we included five manually obtained drill cores of loess-derived slope-wash deposits from the outlet of the valley. We sampled these cores at four depth intervals (40–50 cm, 60–70 cm, 80–90 cm, 90–100 cm). In addition, a purely loess-derived Luvisol 9–10 km west of the valley was included to represent the pure loess in this region. We took 10 samples from 20 cm to 140 cm depth of this profile, each comprising a depth interval of 10–20 cm.

* Correspondence: F. Yang; e-mail: fyang@issas.ac.cn

2.2 Analysis of GSD

Samples were dried at 40°C, homogenized and passed through a 2-mm sieve. Amounts of 0.3 to 0.8 g (depending on estimated clay content) were treated with 0.7 mL 30% hydrogen peroxide (H_2O_2) at 70°C to remove organic matter. The treatment was repeated until the sample was completely bleached. After desiccation, a dithionite–citrate–bicarbonate (DCB) treatment was applied to remove the iron oxides (*Mehra* and *Jackson*, 1960). The suspension was then washed and centrifuged twice with 1 M NaCl solution and twice with deionized water. Prior to grain size analysis, the sample solution was tip-sonicated for 30 s. A Beckmann Coulter LS3320 laser particle size analyzer with polarized intensity differential scattering system (PIDS) was used for grain size measurement. Each sample was analyzed in three cycles à 60 s. The Lorenz-Mie theory was used to calculate the GSD based on the light scattering pattern (*Hergert* and *Wriedt*, 2012). An optical model suitable for quartz (refractive index 1.556, absorption coefficient 0.1) was applied for the calculation (*e.g.*, *Bittelli* et al., 2019). The results were expressed as 116 grain size classes over a range of 0.04–2000 μm.

2.3 Quantification of loess proportions in the slope deposits

As outlined in the results section, GSDs of loess-containing samples were bimodal at most. Therefore, we modified a two-endmembers unmixing model proposed by *Eaqub* and *Blume* (1976) to calculate the proportions of loess in the various slope deposits:

$$Loess\ (\%)\ in\ soil\ sample\ i = (u_i - a)/(b - a) \times 100, \quad (1)$$

where u_i is the proportion of the < 80 μm fraction of sample i, a is the < 80 μm fraction of the sandstone weathering products, and b is the < 80 μm fraction of loess (Fig. 1).

We assumed that the sandstone component of the loess-affected layers was the same as in the loess-free layers (BLs), with the same sandy modal size. Based on the average < 80 μm fraction obtained for the assumed sandstone and loess endmembers, '*a*' was set to 16% for samples with sandy modal sizes in the range of 176–223 μm (Fig. 1a) and to 10% for samples with sandy modal sizes of 234–256 μm (Fig. 1b), '*b*' was set to 96% (Fig. 1).

In addition to the two-endmembers unmixing model, the R package EMMAgeo was applied to decompose the bimodal GSDs of the various layers (*Dietze* and *Dietze*, 2019). In our case, the default setting of the deterministic EMMA function was used. The number of endmembers (parameter q) was set to 2 and the weight transformation limit (l) was set to 0.

3 Results and discussion

3.1 Grain-size distributions of all samples

The samples from different depths of the Luvisol developed in loess showed great similarity in their GSDs, with a common modal size at ≈ 37 μm. Most samples from the BLs also exhibited a unimodal GSD pattern, with modal sizes varying

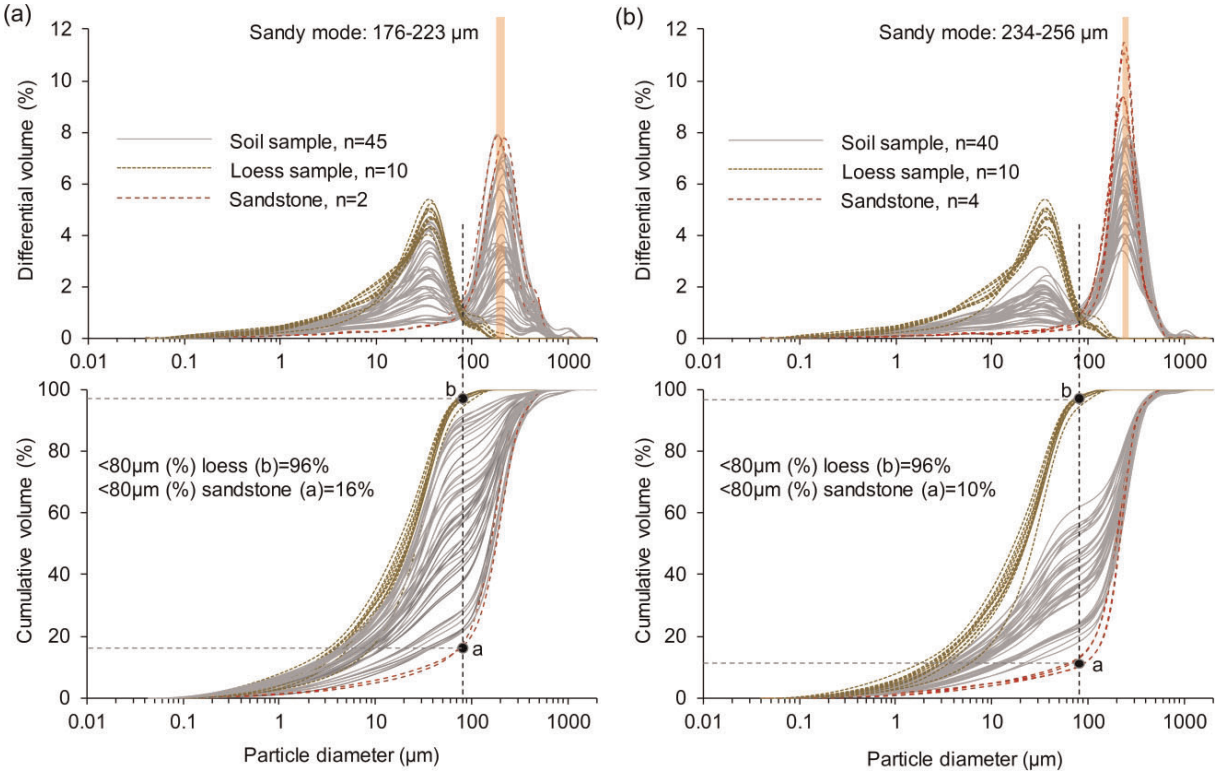

Figure 1: Differential and cumulative GSD curves of all loess-containing samples (grey solid lines), pure loess (brown dotted lines) and loess-free sandstone weathering materials (red dotted lines), (a) for samples with sandy modal sizes in the range 173–223 μm and (b) for samples with sandy modal sizes of 234–256 μm.

from 130 to 340 μm. Almost all samples taken from the layers above the BLs exhibited bimodal GSD patterns. This was also the case for the samples obtained from the drill cores at the outlet of the valley. Two modal sizes, *i.e.*, a silty mode (31–39 μm) and a sandy mode (176–256 μm) apparently corresponded to the modes of loess and sandstone weathering products (constituting the BLs), respectively. GSD curves of loess and loess-free sandstone weathering products from the BLs showed only minor overlap with a turning point at ≈ 80 μm, which was consistent for all loess-containing samples (Fig. 1).

3.2 Performance of the R package EMMAgeo and the two-endmembers unmixing model

The deterministic R package EMMAgeo yielded two nearly unimodal GSD curves, with minor modes resulting from model artefacts (*Dietze* et al., 2012; *Dietze* and *Dietze*, 2019). The two modal sizes at 36 μm and 230 μm (Fig. 2c) matched perfectly with those of loess and sandstone weathering products, respectively (Fig. 1). The two modeled endmembers explained 73% of the class-wise variance (Fig. 2a) and 93% of the sample-wise variance (Fig. 2b) of the dataset. Loess proportions obtained from the EMMAgeo function varied from 0% to 100% (Fig. 2d), which were highly correlated (R^2 = 0.98, n = 85) with those calculated with the two-endmembers unmixing model (Fig. 3). Compared to the two-endmembers unmixing model, EMMAgeo yielded lower loess proportions for samples containing less than about 40% loess and greater loess proportions for samples containing more than about 50% loess (Fig. 3). This result agrees with previous studies in which the EMMA approach tended to underestimate low scores and overestimate high scores (*Dietze* and *Dietze*, 2019). Thus, precaution is recommended in case of extremely high and low scores of one endmember in mixed samples when using the EMMAgeo function.

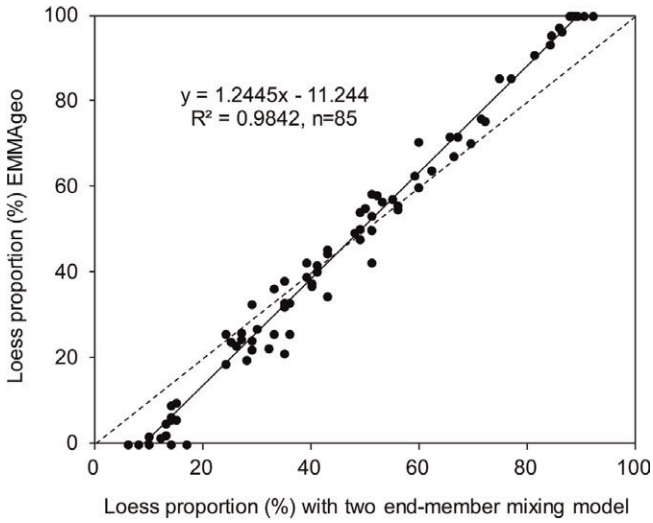

Figure 3: Correlation between loess proportions derived from two-endmembers unmixing model and R function EMMAgeo. The dashed line is the 1:1-line.

3.3 Loess proportions in PPSD and Holocene colluvium

According to the two-endmembers unmixing model, loess proportions of the HCs, ULs, and ILs of the 17 profiles in the

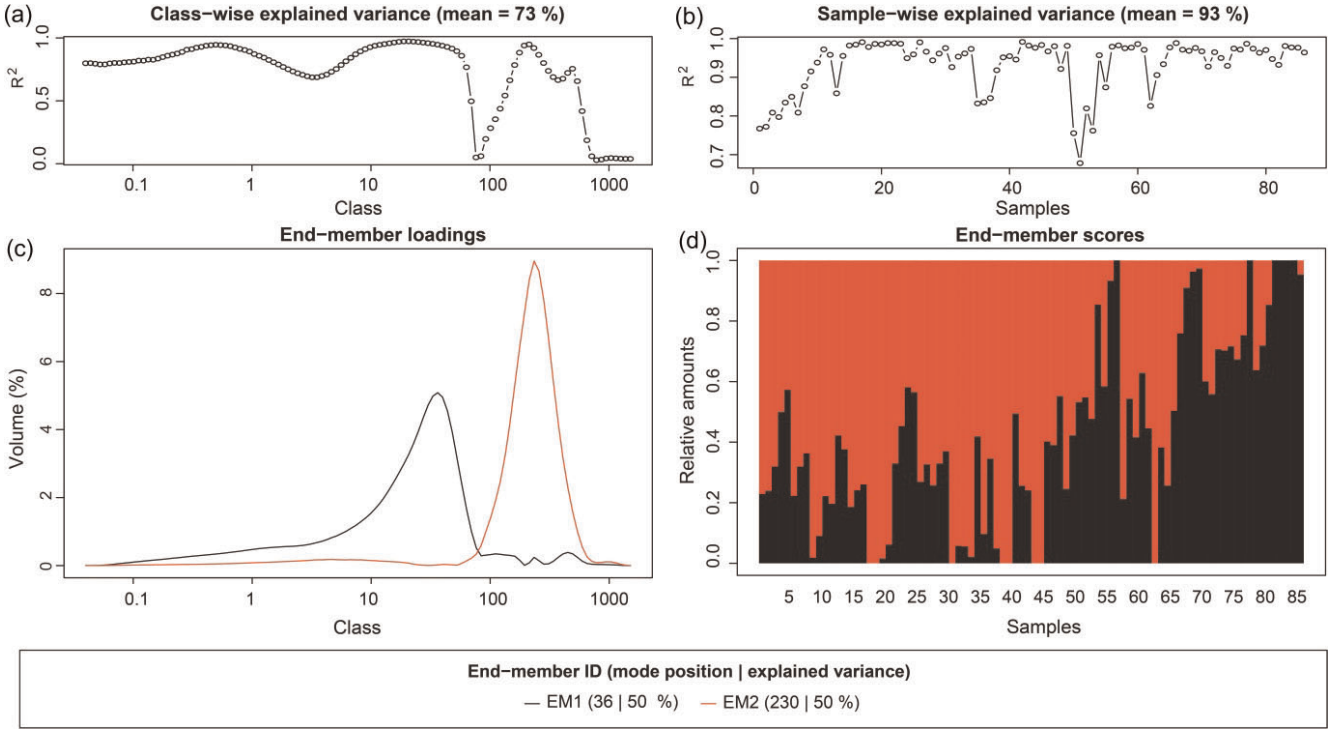

Figure 2: Graphical output of the R function EMMAgeo. (a) Class-wise explained variance (R^2) and (b) sample-wise explained variance (R^2) as measures of model performance, (c) endmember loadings, and (d) endmember scores.

valley varied from less than 10% to more than 90% (Fig. 4). The greatest loess proportions occurred in the ILs (56.9% ± 18.1%, n = 12), which contained about twice as much loess as the HCs (31.1% ± 12.8%, n = 28) and ULs (24.9% ± 12.8%, n = 22). Only samples without any silty mode were considered loess-free, which led to the interpretation that 3 of the 24 analyzed BLs contained a minor loess component (Fig. 4). This is in disagreement to the definition of BLs, which are defined as loess-free solifluction layers. Possible explanations may be (1) a minor silt component in the Buntsandstein layers, (2) an influence by former tree uprooting that is not obvious in the profile morphology anymore, or (3) postdepositional infiltration of silt by percolating soil water (*Kleber* and *Terhorst*, 2013).

Apart from this, our results are in line with vertical patterns of loess proportions in PPSD previously reported from many regions of central Europe (*Kleber* and *Terhorst*, 2013). Loess proportions of the samples from the drill cores at the outlet of the valley were generally higher (averaged 75.3%, n = 20) compared with loess proportions of PPSD within the valley (Fig. 2). We interpret these particularly loess-rich sediments as a product of both, solifluction and sheet-wash on loess-covered slopes. Thereby, solifluction took place in summer, when the active layer had thawed, whereas sheet-wash most likely took place during the initial phase of thawing, when only the upper few centimeters had thawed, leading to surface runoff of the meltwater.

4 Conclusions and outlook

Based on the good agreement of loess proportions obtained by two independent models (EMMAgeo and a simple two-endmembers unmixing model), we conclude that laser-derived GSD data may serve as an effective proxy to quantify loess proportions in sediments and soils. However, it needs to be stressed that the performance of the two-endmembers unmixing models largely depends on the precondition of strong textural contrast between the involved endmembers. In this study, where the endmembers were loess and weathering products of Triassic sandstone, this precondition was perfectly fulfilled. The transferability of this approach to other settings with different boundary conditions strongly depends on the extent to which this precondition is fulfilled there. Compared to the simple two-endmembers unmixing model, EMMAgeo has a broader range of possible applications. It can also be used to identify and quantify subpopulations of mixed samples with more than two endmembers that are sufficiently distinct from each other (*Dietze* and *Dietze*, 2019). Yet, geological background information is essential for correct interpretation of genetically meaningful grain-size endmembers when applying EMMAgeo (*Dietze* and *Dietze*, 2019).

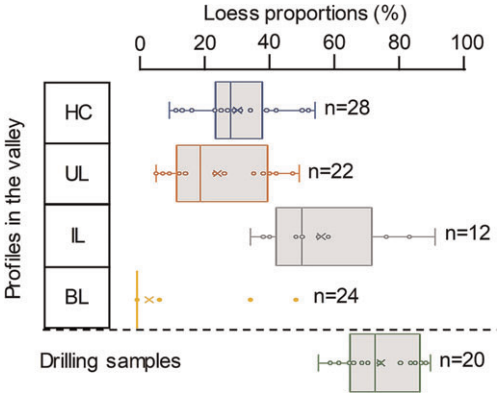

Figure 4: Loess proportions (calculated by two-endmembers unmixing model) of Holocene colluvium (HC), Upper Layer (UL), Intermediate Layer (IL), and Basal Layer (BL) from 17 profiles along the valley and of loess-derived slope-wash deposits from drill cores at the outlet of the valley.

For the first time, we were able to use GSD data for quantifying loess proportions in PPSD and HCs across a landscape. This important step will allow for assessing the spatial patterns of loess proportions in PPSD and HCs as a function of relief, and for quantifying the pedological and ecological effects of various loess proportions.

Acknowledgments

This work is supported by the *CSC-DAAD Postdoc Scholarship, by the Joint Committee of the Sino-German Center for Research Promotion (M-0046)*, and by the *Chinese Academy of Sciences (151432KYSB20190004)*. We thank *Nora Pfaffner, Marius Friedrich, Tino Peplau* and several students for their assistance in the field, and *Cornelia Friedrich* for her help with the grain size analysis. We thank *Michael Dietze* for modifying the EMMAgeo codes. We thank *Xiaorui Zhao* and *Jun Gu* for generating Fig. 2. Special thanks to *Arno Kleber* and two anonymous reviewers for their comments helping to improve the manuscript.

References

AK Bodensystematik (1998): Systematik der Böden und der Bodenbildenden Substrate Deutschlands. *Mitt. Dt. Bodenkundl. Ges.* 86, 180–180.

Bittelli, M., *Andrenelli, M. C.*, *Simonetti, G.*, *Pellegrini, S.*, *Artioli, G.*, *Piccoli, I.*, *Morari, F.* (2019): Shall we abandon sedimentation methods for particle size analysis in soils? *Soil Till. Res.* 185, 36–46.

Dietze, E., *Dietze, M.* (2019): Grain-size distribution unmixing using the R package EMMAgeo. *E&G Quat. Sci. J.* 68, 29–46.

Dietze, E., *Hartmann, K.*, *Diekmann, B.*, *IJmker, J.*, *Lehmkuhl, F.*, *Opitz, S.*, *Stauch, G.*, *Wuennemann, B.*, *Borchers, A.* (2012): An end-member algorithm for deciphering modern detrital processes from lake sediments of Lake Donggi Cona, NE Tibetan Plateau, China. *Sediment. Geol.* 243, 169–180.

Eaqub, M., *Blume, H. P.* (1976): Soil development on sandstone solifluction deposits with varying contents of loess materials. *Catena* 3, 17–27.

Hergert, W., *Wriedt, T.* (2012): The Mie Theory: Basics and Applications. Springer, Berlin, Germany.

Kleber, A. (2006): "Kolluvium" does not equal "colluvium". *Z. Geomorph.* 50, 541–542.

Kleber, A. (1997): Cover-beds as soil parent materials in midlatitude regions. *Catena* 30, 197–213.

Kleber, A., *Terhorst, B.* (2013): Mid-Latitude Slope Deposits (Cover Beds). Elsevier, Amsterdam, The Netherlands.

Krautz, J., *Gärtner, A.*, *Hofmann, M.*, *Linnemann, U.*, *Kleber, A.* (2018): Cover beds older than the mid-pleistocene revolution and the provenance of their eolian components, La Sal Mountains, Utah, USA. *Quat. Sci. Rev.* 185, 1–8.

Mailänder, R., *Veit, H.* (2001): Periglacial cover-beds on the Swiss Plateau: indicators of soil, climate and landscape evolution during the Late Quaternary. *Catena* 45, 251–272.

Mehra, O. P., *Jackson, M. L.* (1960): Iron oxide removal from soils and clays by dithionite–citrate system buffered with sodium bicarbonate. *Clay. Clay Miner.* 7, 317–327.

Paterson, G. A., *Heslop, D.* (2015): New methods for unmixing sediment grain size data. *Geochem. Geophys. Geosyst.* 16, 4494–4506.

Raab, T., *Leopold, M.*, *Völkel, J.* (2007): Character, age, and ecological significance of Pleistocene periglacial slope deposits in Germany. *Phys. Geogr.* 28, 451–473.

Sauer, D., *Felix-Henningsen, P.* (2004): Application of ground-penetrating radar to determine the thickness of Pleistocene periglacial slope deposits. *J. Plant Nutr. Soil Sci.* 167, 752–760.

Semmel, A., *Terhorst, B.* (2010): The concept of the Pleistocene periglacial cover beds in central Europe: A review. *Quat. Int.* 222, 120–128.

Sun, D., *Bloemendal, J.*, *Rea, D. K.*, *Vandenberghe, J.*, *Jiang, F.*, *An, Z.*, *Su, R.* (2002): Grain-size distribution function of polymodal sediments in hydraulic and aeolian environments, and numerical partitioning of the sedimentary components. *Sediment. Geol.* 152, 263–277.

Waroszewski, J., *Sprafke, T.*, *Kabała, C.*, *Kobierski, M.*, *Kierczak, J.*, *Musztyfaga, E.*, *Lobaa, A.*, *Mazureke, R.*, *Łabaz, B.* (2019): Tracking textural, mineralogical and geochemical signatures in soils developed from basalt-derived materials covered with loess sediments (SW Poland). *Geoderma* 337, 983–997.

Weltje, G. J. (1997): End-member modeling of compositional data: Numerical-statistical algorithms for solving the explicit mixing problem. *Math. Geol.* 216, 503–549.